A plasmon-assisted fluoro-immunoassay using gold nanoparticle-decorated carbon nanotubes for monitoring the influenza virus

A Plasmon-Assisted Fluoro-Immunoassay using Gold Nanoparticle-Decorated Carbon Nanotubes for Monitoring the Influenza Virus

Jaewook Lee[1,5], Syed Rahin Ahmed[2,3], Sangjin Oh[3], Jeonghyo Kim[3], Tetsuro Suzuki[4], Kaushik Parmar[5], Simon S. Park[5], Jaebeom Lee[3,*], and Enoch Y. Park[1,2,*]

[1]Research Institute of Green Science and Technology, Shizuoka University 836 Ohya Suruga-ku, Shizuoka 422-8529, Japan

[2]Department of Bioscience, Graduate School of Science and Technology, Shizuoka University, 836 Ohya Suruga- ku, Shizuoka 422-8529, Japan

[3]Department of Nano Fusion and Cogno-Mechatronics Engineering, Pusan National University, Busan 609-735, Korea

[4]Department of Infectious Diseases, Hamamatsu University School of Medicine, 1-20-1 Higashi-ku, Handa-yama, Hamamatsu 431-3192, Japan

[5]Department of Mechanical and Manufacturing Engineering, University of Calgary, Calgary, T2N 1N4, Canada

[*]Address correspondence to acypark@ipc.shizuoka.ac.jp (EYP) and jaebeom@pusan.ac.kr (JL).

ABSTRACT

A plasmon-assisted fluoro-immunoassay (PAFI) was developed for the detection of the influenza virus by using Au nanoparticle (Au NP)-decorated carbon nanotubes (AuCNTs) that were synthesized using phytochemical composites at room temperature in deionized water. Specific antibodies (Abs) against the influenza virus were conjugated onto the surface of AuCNTs and cadmium telluride quantum dots (QDs), which had a photoluminescence intensity that varied as a function of virus concentration and a detection limit of 0.1 pg/mL for all three types of influenza viruses examined. The clinically isolated influenza viruses (A/Yokohama/110/2009 (H3N2)) were detected in the range of 50–10,000 PFU/mL, with a detection limit of 50 PFU/mL. From a series of proof-of-concept and clinical experiments, the developed PAFI biosensing system provided robust signal production and enhancement, as well as an excellent selectivity and sensitivity for influenza viruses. This nanoparticle-based technique could be potentially developed as an efficient detection platform for the influenza virus.

KEYWORDS: Plasmon-assisted fluoro-immunoassay, Gold nanoparticle-decorated carbon nanotube, CdTe quantum dot, Influenza virus detection platform, Plasmonic resonance energy transfer

1. Introduction

Many kinds of nanomaterials have been recently used in the area of nanobiotechnology research. The unique physicochemical properties of nanomaterials have found a significant number of applications in biosensing, imaging, and drug delivery system (Ahmed et al. 2013; Lee et al. 2014; Leung et al. 2012; Li and Mezzenga, 2013; Wang et al. 2013b). In particular, nanobiosensing systems have gained popularity owing to its high sensitivity, selectivity, and rapid response time (Liu et al. 2012; Yin et al. 2013). The detection techniques used in various nanobiosensing applications include magnetophoresis, electrochemical analysis, plasmonic coupling immunoassays, and fluoro-immunoassays (Draz et al. 2012; Kim et al. 2013; Li et al. 2013; Viet et al. 2013; Zhou et al. 2012; Zhou et al. 2013). The plasmon-assisted fluoro-immunoassay (PAFI) has been used to analyze specific biomaterials (Ahmed et al. 2014; Li et al. 2012; Nooney et al. 2010; Sharma et al., 2013b). The PAFI is based on the plasmonic resonance energy transfer (PRET) phenomenon, which causes a photoluminescence (PL) enhancement from the interactions between the plasmonic nanomaterials and the semiconductor nanoparticles (Lee et al. 2004; Lee et al. 2005; Lee et al. 2007). Such hybrid structures can be used to detect the interaction between an antibody (Ab) and its antigen, because of their tuned optical properties. Although numerous plasmonic nanomaterials have been introduced (*e.g.*, gold, silver, platinum, and metal NPs), Au NP-decorated carbon nanotubes (AuCNTs) have received considerable attention, owing to their unique properties. Au NPs are able to exhibit surface plasmon resonance (Jana et al. 2001; Lee et al. 2011b). Carbon nanotubes exhibit electroconductivity and harbor many π electrons on their surfaces (Jariwala et al.

2013; Sun et al. 2011). Thus, AuCNTs are expected to show a synergistic effect owing to their roles as biosensing platforms, signal enhancers, and signal transducers (McAndrew and Baxendale, 2013; Sharma et al. 2013a; Wang et al. 2013a; Yick et al. 2013).

Combining the above mentioned heterogeneous materials requires sophisticated strategies in order to conserve carbon nanotube (CNT) structures and to bind two materials without the help of organic bridges. One of the well-known processes for preparing AuCNT nanostructures involves reduction with chemical reducing agents such as sodium borohydride or hydrazine (Yu et al. 2014; Zhang et al. 2013). An alternative process involves thiol- or amine-assisted interactions between Au NPs and CNT surfaces (Georgakilas et al. 2007; Li et al. 2011). Attachment of Au NPs onto CNT surfaces has been attempted using the processes of electrodeposition, DNA hybridization, and chemical reaction (Georgakilas et al. 2007; Gobbo et al. 2013; Li et al. 2011; Li and Cooper-White, 2013; Peng et al. 2009). However, these approaches can cause CNT damage and organic/biological electric resistance, which may adversely affect their electrical and mechanical properties (Hirsch, 2002; Holzinger et al. 2001).

In this study, we suggest a novel and easy method for preparing AuCNTs by using phytochemicals. The synthetic reaction was carried out in deionized (DI) water at room temperature *via* sonication and stirring processes, without resorting to external heating or application of high pressure. No electrochemistry equipment was used in the above procedure. AuCNTs were produced as follows. Au ions were first attached onto the surface of CNTs and they were then reduced to Au NPs on the CNT surface. This process was catalyzed using a mixture of gallic acid and isoflavone phytochemicals, two well-known natural antioxidants (Aruoma et al. 1993;

Park et al. 2009) that served as mild reducing agents (Lee et al. 2011a). Furthermore, the generated AuCNTs were applied onto the influenza virus detection platform by using a quantum dot (QDs)-assisted PAFI.

In this study, we developed a PAFI-based detection platform for the influenza virus, using antibody-conjugated AuCNTs and CdTe QDs. In all, we tested three types of influenza viruses, *viz*. the Influenza virus A/Beijing/262/95 (H1N1), the Influenza virus/New Caledonia/20/99IvR116 (H1N1), and the clinically isolated Influenza virus A/Yokohama/110/2009 (H3N2). The minimum detection limit for the influenza virus was 0.1 pg/mL. The clinically isolated influenza virus was also monitored in the range 50–10,000 PFU/mL, with a detection limit of 50 PFU/mL. Our virus detection platform would be immensely useful not only for detecting the influenza virus, but also for detecting various other viruses and viral diseases.

2. Material and methods

2.1. Materials and instruments

$HAuCl_4 \cdot 3H_2O$, multi-walled carbon nanotubes (MWCNTs), gallic acid, EDC, NHS, cadmium perchlorate hydrate, and cysteamine were purchased from Sigma-Aldrich (Milwaukee, WI, USA). Aluminum telluride (Al_2Te_3) was obtained from the Cerac Company (Milwaukee, WI, USA). The isoflavone was isolated from commercial soybeans. 3,3′,5,5′-tetramethylbenzidine was purchased from Dojindo (Osaka, Japan). The ECL™ anti-mouse IgG, horseradish peroxidase (HRP)-conjugated whole antibody (Ab) was obtained from GE Healthcare UK, Ltd. (Buckinghamshire, UK). Goat anti-rabbit IgG-HRP was purchased from Santa Cruz Biotechnology, Inc. (Santa Cruz, CA, USA). Anti-Influenza A virus hemagglutinin (HA) Ab Ab66189,

110 which is a mouse monoclonal antibody [B219M] for the influenza A virus HA H1 and
111 positive against influenza virus A/Beijing/262/95 (H1N1), A/New Caledonia/20/99
112 (H1N1), and A/Taiwan/1/86 (H1N1), was purchased from Abcam Inc. (Cambridge,
113 UK). Anti-neuraminidase (NA) (New Caledonia/20/1999/(H1N1)), a rabbit polyclonal
114 Ab, was obtained from Immune Technology Corp. (New York, NY, USA). Anti-H3
115 (H3N2) (Ab82454), a mouse monoclonal Ab [InA227] to H3 (H3N2) that recognizes
116 influenza virus A HA H3, was purchased from Abcam Inc. (Cambridge, UK).
117 Influenza virus New Caledonia/20/99IvR116 (H1N1) and A/Beijing/262/95 (H1N1)
118 were purchased from Sino Biological Inc. (Beijing, China) and HyTest Lyd (Turku,
119 Finland), respectively. Influenza virus A/Yokohama/110/2009 (H3N2) was isolated
120 from a clinically isolated sample, which was kindly provided by Dr. C. Kawakami of
121 Yokohama City Institute of Health, Japan and was used to assess the versatility of
122 this assay system.

123 The absorbance of AuCNTs and the corresponding PL enhancement were
124 measured using a filter-based multimode microplate reader (Infinite® F500, TECAN,
125 Ltd., Männedorf, Switzerland), and the chemical reactions and surface functional
126 groups were monitored by FT-IR spectroscopy (FT-IR 6300, JASCO, Corp. Tokyo,
127 Japan). The morphologies and sizes of the nanostructures were characterized by
128 TEM (JEM-2100F, JEOL, Ltd., Tokyo, Japan). An X-ray powder diffractometer (RINT
129 ULTIMA, Rigaku, Corp., Tokyo, Japan) was used to characterize AuCNT by using
130 CuKa radiation and a Ni filter. The data were collected from 2 theta = 0–100° at a
131 scan rate of 0.01° per step and 10 s per point. The AuCNTs and MWCNTs were
132 analyzed by Raman spectroscopy (HR-800, LabRAM, HORIBA Ltd., Kyoto, Japan).
133 In order to measure the electroconductivity, AuCNT solution was dropped on the
134 planar interdigitated electrode (planar IDE-Pt/0.25", Synkera, USA) and dried at

135 room temperature. Then, the current change of the deposited area was monitored by
136 linear sweep voltammetry from -1 V to 1 V (SP-150, BioLogic, France). A plate
137 reader (Model 680, Bio-Rad, Hercules, USA) was used to confirm the presence of
138 Ab-conjugated nanomaterials. The PL image of the hybrid nanostructure was
139 observed using a confocal laser-scanning microscope (LSM 700, Carl Zeiss
140 Microimaging, GmbH, Göttingen, Germany).
141
142 *2.2. Synthesis of AuCNTs and CdTe QDs*
143 AuCNTs were synthesized at room temperature by using commercially available
144 reagents. Forty milligrams of MWCNT was dispersed in 100 mL of nitric acid and
145 boiled for 5 h to prepare the hydrophilic MWCNTs. Subsequently, 0.01 mmol of
146 $HAuCl_4 \cdot 3H_2O$ and 2 mg of acid-treated MWCNTs were dispersed in 30 mL of DI
147 water by sonication for 30 min. Subsequently, 600 μL of GI solution was added into
148 the MWCNT/Au ion solution, and then stirred vigorously for 1 h. The GI solution was
149 used as a reducing agent and stabilizer, and prepared as follows: 10 mg of
150 isoflavone was dissolved in 10 mL of the 0.01 M gallic acid solution. The cysteamine-
151 coated CdTe QDs were synthesized as reported in detail elsewhere (Gaponik et al.
152 2002; Lee et al. 2010).
153
154 *2.3. Preparation of antibody-conjugated AuCNTs and CdTe QDs*
155 In order to conjugate the Abs to the AuCNTs, amine-functionalized AuCNTs and
156 Ab-conjugated EDC/NHS were prepared. To modify the surface of the Au NPs, 1 mg
157 of AuCNTs was dispersed in 10 mL of DI water. Then, 1 mL of 0.01 M cysteamine
158 was added into the AuCNT solution. After 30 min of stirring, this mixture was
159 centrifuged to separate the amine-functionalized AuCNTs. Additionally, 100 μL of the

160 4 mM EDC and 10 mM NHS were added in the 96-well plate and incubated and
161 gently shaken for 30 min at 200 rpm with 1 μL of anti-HA Ab (Ab66189) (final
162 concentration of 5 ng/mL) for the EDC/NHS coupling reaction. Finally, 30 μL of the
163 amine-functionalized AuCNT (1 μg/μL) and activated anti-HA Ab (Ab66189) were
164 mixed in all wells and shaken for 3 h for effective bioconjugation. Anti-NA (New
165 Caledonia/20/1999/(H1N1)) and anti-HA (Ab82454) Abs were also conjugated to the
166 surfaces of the Au CNTs by using the same procedure. Anti-HA (Ab66189) and anti-
167 HA (Ab82454)-conjugated CdTe QDs were also prepared by using the procedure for
168 Ab-conjugated AuCNTs.
169
170 *2.4. Plasmon assisted fluoro-immunoassay (PAFI) for influenza virus detection*
171 In order to detect the influenza virus *via* PAFI, 45 μL of Ab-conjugated AuCNTs
172 and 45 μL of the CdTe QDs were mixed in each of the 96 wells. Consequently,
173 serially diluted influenza virus was added into each well and shaken for 1 h. During
174 this process, the Ab-conjugated AuCNTs and the CdTe QDs were found to bind each
175 other in the presence of the influenza virus, owing to the affinity between the antigen
176 on the surface of virus and its corresponding antibody. To evaluate the efficacy of
177 PAFI as a detection platform, the following three types of influenza viruses were
178 used: A/Beijing/262/95 (H1N1), New Caledonia/20/99IvR116 (H1N1), and
179 A/Yokohama/110/2009 (H3N2). The PL intensities were measured as a function of
180 the concentration of the influenza virus. The PAFI was carried out at an excitation
181 wavelength of 380 nm, and the excitation and the emission slits were 5 and 10 nm in
182 width, respectively. The PL intensity of this system was monitored at 518 nm during
183 signal detection. In order to evaluate the PAFI system with different influenza virus,
184 all detection experiment was carried out over 3 times.

3. Results and Discussion

3.1. Design and preparation of AuCNTs for PAFI

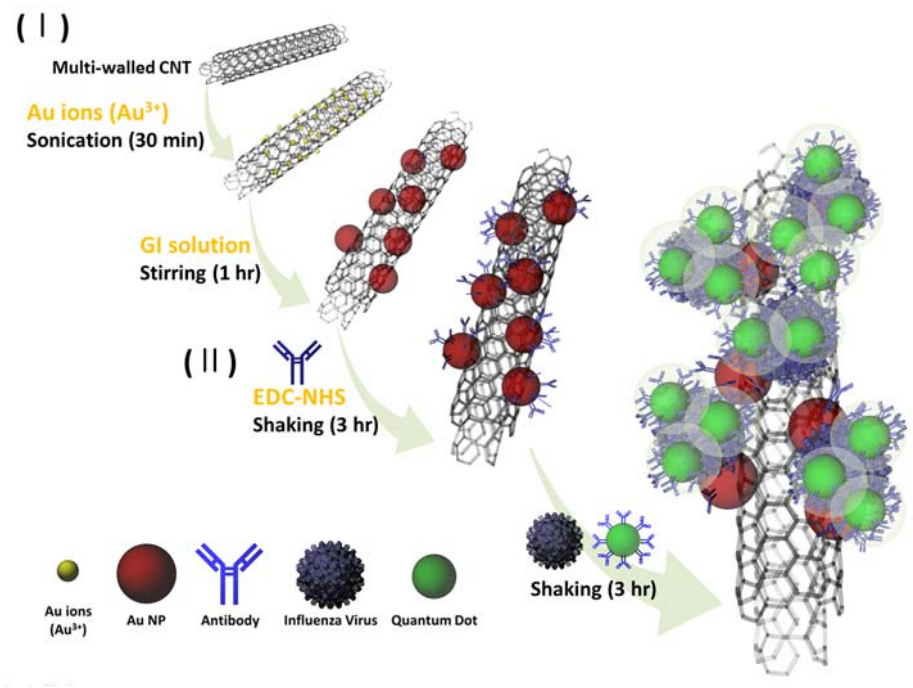

Fig. 1. (I) Synthetic scheme for the preparation of Au nanoparticle (NP)-decorated CNT nanostructures (AuCNTs) and (II) the process of influenza virus detection by using PAFI, non-scalable.

The synthesis of AuCNTs comprised two steps (Fig. 1), *viz*. the preparation of plasmonic nanomaterials (step I), and the processing of PAFI for influenza virus detection by using AuCNTs and QDs (step II). Firstly, the acid-treated multi-walled CNTs (MWCNTs) were dispersed in DI water containing a gold precursor (Au^{3+}) by using sonication. Owing to the π-electrons and oxygen moieties on the surface of the acid-treated MWCNTs, Au^{3+} is able to attach onto the surface of MWCNTs through

electrostatic attraction. In order to decorate Au NPs onto the MWCNTs, the Au ions were reduced to Au NPs, using a mixture of gallic acid and isoflavone (GI solution). AuCNTs were obtained after 1 h of stirring and washing with DI water. To perform the PAFI for influenza virus detection by using AuCNTs, anti-hemagglutinin (HA) Ab or anti-neuraminidase (NA) Ab specific for the influenza virus were conjugated onto the surfaces of AuCNTs and QDs by using a *N*-ethyl-*N′*-(dimethylaminopropyl) carbodiimide (EDC)/*N*-hydroxysuccinimide (NHS)-coupling reaction (step II in Fig. 1). In the presence of the influenza virus, the distance between the Ab-conjugated AuCNTs and the QDs diminishes by an affinity between an antigen and its Ab. Depending on the concentration of the influenza virus, the formation of the AuCNT and QD hybrid structures caused a variation in the PL intensities. In the PAFI system, plasmonic material is not single Au NP but AuCNT assembly structure. Thus the energy transfer to enhance the PL property would be taken a place at the sandwich structure between plasmonic AuCNT structure and fluorescent CdTe QDs with virus. Moreover, this sandwich structure could lead the PL enhancement through the collective effect between plasmonic materials and fluorescent nanoparticles (Lee at al. 2004).

3.2. Morphology of AuCNTs

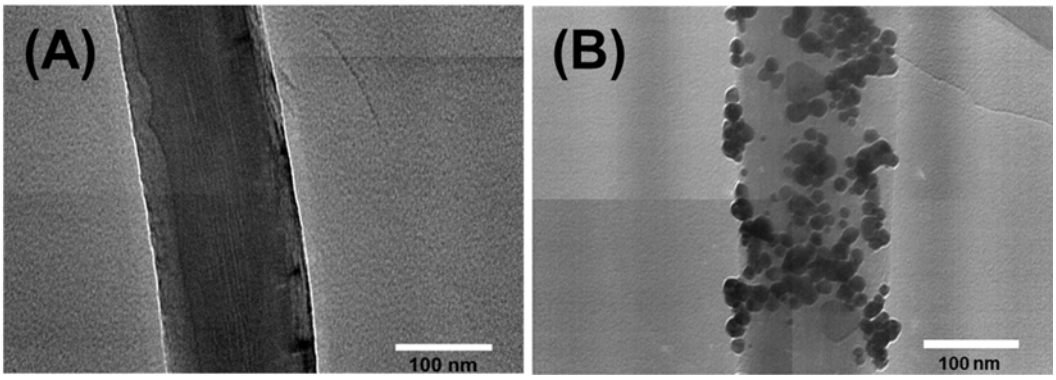

Fig. 2. TEM images of (A) MWCNTs and (B) AuCNTs.

In order to confirm the decoration of Au NPs onto MWCNTs, the morphology of MWCNTs and AuCNTs were examined using transmission electron microscopy (TEM). The MWCNTs showed the presence of a slick surface that was over 3 μm in length (Fig. 2A and Fig. S1A, respectively). However, after two steps of the decoration reaction, a large number of Au NPs were detected on the surface of MWCNTs (Fig. 2B and Fig. S1B). The carbon structure of MWCNT is transparent, but as heavy metals show high electron absorption, Au NPs are easily distinguishable in the TEM images. The average particle size of the Au NPs was 20 nm, and they were well dispersed with a high density over the large surface area of the MWCNTs (Fig. S1B).

3.3. Optical, surface-enhanced Raman scattering*, physicochemical, and electrical properties of AuCNTs*

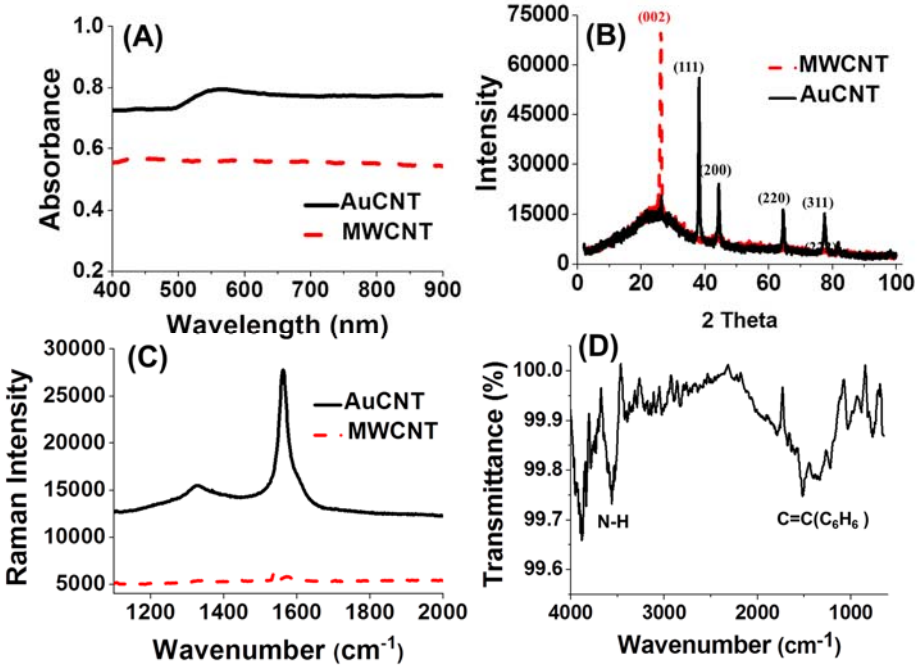

Fig. 3. Physicochemical properties of the AuCNTs. (A) UV/Vis spectra, (B) XRD data, (C) Raman spectra of MWCNT with Au ions (red dash line) and AuCNTs (black line), and (D) FT-IR spectra of the amine-functionalized AuCNTs.

The optical absorbance of AuCNTs was measured using a filter-based absorbance-mode microplate reader. Typically, the plasmon peak of Au NPs that are 20 nm in radius occurs at 525 nm. However, the surface plasmonic absorbance of Au NPs was observed as a black spectrum at 550 nm (Fig. 3A), and its bands were broadened and non-symmetric; however, large-sized (>50 nm) particles were not observed in the corresponding TEM image. Plasmon-coupling between adjacent Au NPs might have occurred, owing to the delocalized π-electron cloud on the surface of MWCNTs. This interaction caused a broadened and non-symmetric plasmonic band of Au NPs. Thus MWCNT can play a role as mediator for plasmonic coupling interaction, thus optical property of this hybrid structure could be enhanced (Lee et al. 2012). However, in the MWCNT case, the specific absorbance as plasmonic peak was not observed by UV/Vis spectroscopy. Thus, only MWCNT was not suitable for

252 PAFI detection platform. The structural characteristics of the AuCNTs were
253 elucidated based on the powder X-ray diffraction (XRD) pattern (Fig. 3B). A strong
254 diffraction peak corresponding to the 002 plane of the MWCNTs was presented at 2
255 theta = 26.2° in the XRD pattern (ICSD card no: 01-075-1621). Meanwhile, several
256 new diffraction patterns and weak carbon peaks were measured in the AuCNTs (Fig.
257 3B, red pattern). The presence of Au NPs in the nanostructure was confirmed by the
258 characteristic diffraction peaks from the face-centered cubic packing arrangement of
259 bulk Au *i.e.*., the (111), (200), (220), (311), (222), and (400) planes at 2 theta values
260 of 38.2°, 44.4°, 64.6°, 77.5°, 81.7°, and 98.1° (ICSD card no: 00-004-0784),
261 respectively. Au NPs possess a higher crystallinity than the carbon structures,
262 because of the metal NPs. Thus, the diffraction patterns of Au NPs were stronger
263 than those of the carbon face. The surface-enhanced Raman scattering (SERS) was
264 measured by Raman spectroscopy at the excitation wavelength of 514 nm (Fig. 3C).
265 The peak at 1340 cm^{-1} indicates that the D band occurred due to the local disorder
266 present in the AuCNT structure (Sharma et al. 2013a). In addition, a G peak
267 appeared near 1580 cm^{-1}, which is related to the characteristic feature (especially to
268 the sp2-hybridized carbon allotropes) of the graphitic layers (Baro et al. 2013). As
269 expected, the Raman spectrum intensity was more enhanced in the AuCNTs than in
270 the MWCNTs (Sharma et al. 2013a) The spectrum intensity of AuCNTs was 5 times
271 higher than that of MWCNTs. Therefore, the SERS effect was induced by decoration
272 of Au NPs onto the MWCNT surface. The functional group of the amine-
273 functionalized AuCNT was analyzed using Fourier Transform Infrared (FT-IR)
274 spectroscopy. For the EDC/NHS coupling reaction with the carboxylic group of the
275 influenza virus antibody, the N-H vibration of AuCNT was detected around 1250 cm^{-1}
276 and 3400–3500 cm^{-1} (Fig. 3D), respectively. These bands around 1450–1580 cm^{-1}

277 are characteristic of the aromatic bonds of MWCNT. The C–O single-bond vibration
278 was observed at 1010 cm^{-1}. The electroconductivities of the AuCNTs and MWCNTs
279 were measured using a finger type Pt electrode *via* the linear sweep method. The
280 average linear resistance of AuCNT was approximately 0.007 mΩ, whereas that of
281 MWCNT was much higher (Fig. S2). From these physicochemical results, it was
282 evident that the AuCNT composite exhibits enhanced properties such as SERS and
283 electrical conductivity. Furthermore, we could experimentally establish the fact that
284 critical damage to the AuCNT structure indeed did not occur, and that AuNPs were
285 directly attached onto the surface of the CNTs, owing to a mild reduction reaction.
286

287 *3.4. PAFI performance for influenza virus detection by using AuCNT*

288 In order to assess the PAFI performance for the influenza virus detection, three
289 types of antibodies, *viz*. anti-HA (H1) (Ab66189), anti-neuraminidase (NA) (New
290 Caledonia/20/1999/(H1N1)), and anti-HA (H3N2) (Ab82454) were conjugated onto
291 the surface of AuCNTs (step II in Fig. 1). In addition, the surfaces of CdTe QDs were
292 also conjugated with anti-HA (H1) (Ab66189) and anti-HA (H3N2) (Ab82454)
293 antibodies by using the same method. In this case, the Ab-conjugated AuCNTs play
294 the role of plasmon-supplying substrates, whereas the Ab-conjugated CdTe QDs act
295 as PL-monitoring materials. Prior to virus detection, conjugation of the Abs to the
296 AuCNTs or CdTe QDs was verified using an ELISA (Figure S3). Anti-HA (Ab66189)
297 and anti-NA (New Caledonia/20/1999/ (H1N1))-conjugated AuCNTs, and anti-HA
298 (Ab66189)-conjugated CdTe QDs displayed strong signals (Fig. S3A, B, and C,
299 respectively). In the case of the anti-HA (Ab82454)-conjugated AuCNTs and the
300 CdTe QDs, the recorded absorbance was lower than that of the other Ab-conjugated
301 NPs (Fig. S4). These results indicate that all antibodies were successfully

conjugated onto the surface of the AuCNTs and the CdTe NPs.

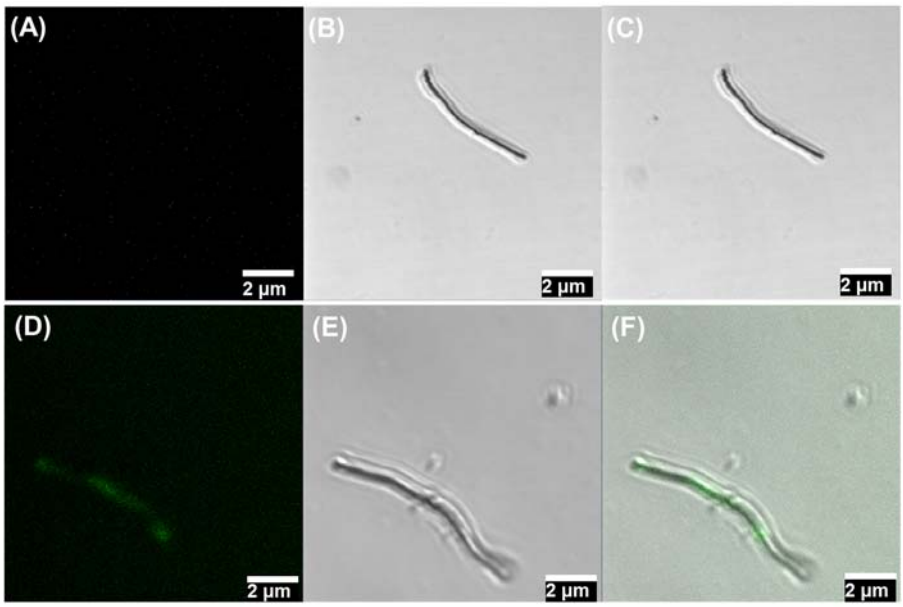

Fig. 4. Confocal laser-scanning microscopy images of the AuCNT-QD hybrid structure obtained via the anti-HA Ab conjugation reaction with influenza virus A/Beijing/262/95 (H1N1). (A)–(C) Before and (D)–(F) after the conjugation reaction with influenza virus. (A) and (D) are fluorescent images; (B) and (E) are DIC images; (C) and (F) are merged images.

The Ab-conjugated nanostructures were used for constructing the PAFI system. The detection of the influenza virus was made possible by using a confocal laser-scanning microscope (Fig. 4). Influenza virus A/Beijing/262/95 (H1N1) was dosed into the anti-HA Ab-conjugated AuCNTs and onto the CdTe system. In the presence of the virus, the distance between the HA Ab-conjugated AuCNTs and the HA Ab-conjugated CdTe QDs was reduced, owing to the affinity between the antigen on the surface of the virus and conjugated antibody. Subsequently, the hybrid nanowire structure showed green PL (Fig. 4D–F). However, no PL was observed at all in the absence of the virus (Fig. 4A–C).

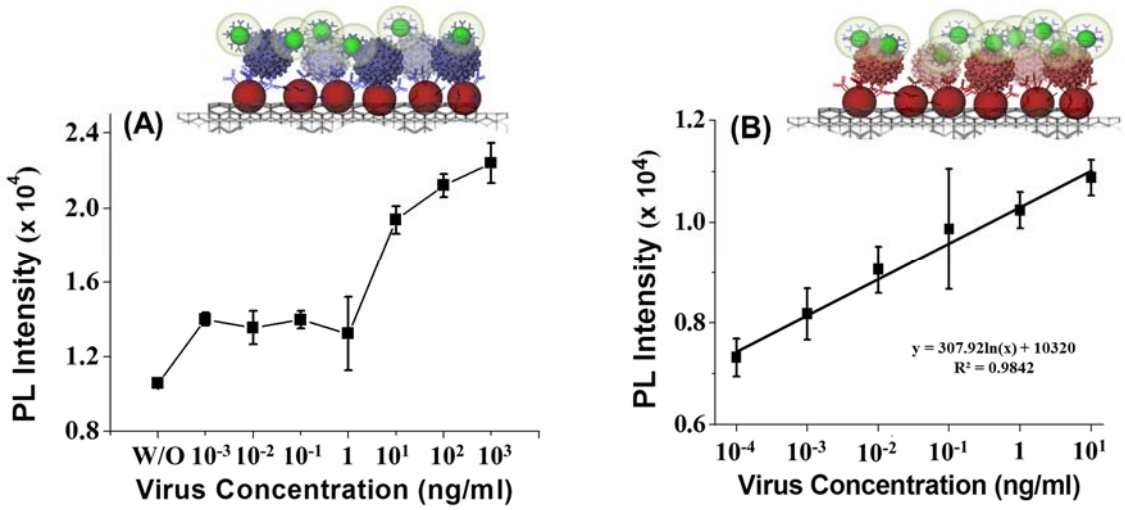

Fig. 5. The calibration curve of the PL intensity corresponding to the concentration of (A) Influenza virus A/Beijing/262/95 (H1N1) and (B) Influenza virus/New Caledonia/20/99IvR116 (H1N1).

In addition, the sensitivity of the PAFI was demonstrated with two different influenza viruses; A/Beijing/262/95 (H1N1) and New Caledonia/20/99IvR116 (H1N1), respectively. All procedures were carried out in a 96-well plate. As the concentration of the influenza virus was increased, the PL intensity corresponding to both of the viruses also increased (Fig. S5). This implies that the binding affinity between the Ab-conjugated AuCNTs and the CdTe QDs was dependent on the virus concentration. Furthermore, using anti-HA Ab (Ab66189)-conjugated AuCNTs and CdTe QDs, we carried out the PAFI for the influenza virus A/Beijing/262/95 (H1N1). The detection was carried out at 518 nm, and a calibration curve corresponding to the virus concentrations was obtained (Fig. 5A). In this case, the detection limit was 1 ng/mL. As the same antibody was conjugated onto the surface of both the nanomaterials, a binding competition took place between the Ab-conjugated AuCNTs and the CdTe QDs against virus. To improve the detection limit of PAFI, various different antibodies were conjugated onto the surface of each of the nanomaterials: anti-NA Ab (New

338 Caledonia/20/1999/(H1N1))-conjugated AuCNTs and anti-HA Ab (Ab66189)-
339 conjugated CdTe QDs (Fig. 5B, anti-NA Ab; red color Ab and anti-HA Ab; blue color
340 Ab). Using these two different nanostructures the influenza virus/New
341 Caledonia/20/99IvR116 (H1N1) was monitored at the same PL emission wavelength.
342 The calibration curve shows a more reliable linearity than that with the same Ab-
343 conjugated system (Fig. 5B). The sensitivity was more improved, and the detection
344 limitation was 0.1 pg/mL.

345

346 *3.5. Detection of the clinically isolated Influenza virus*

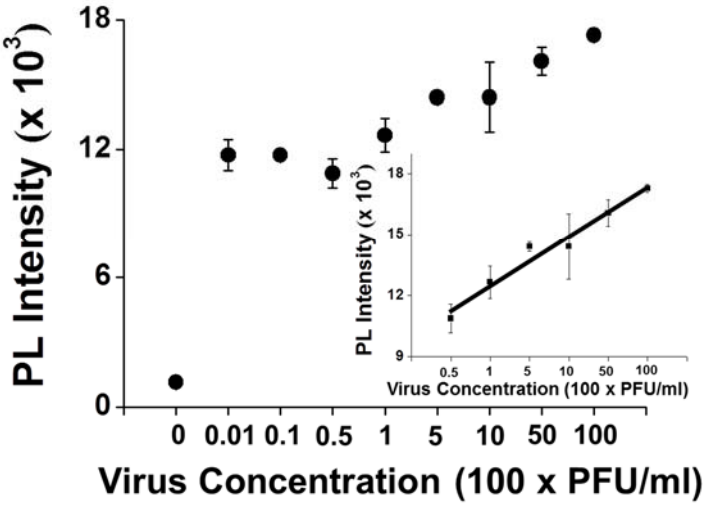

347

348 **Fig. 6.** The calibration curve of the clinically isolated influenza virus A/Yokohama/110/2009
349 (H3N2).

350

351 The clinically isolated sample (influenza virus A/Yokohama/110/2009 (H3N2))
352 was also detected by PAFI using the anti-HA Ab (Ab82454)-conjugated AuCNTs and
353 CdTe QDs at 518 nm in the 96-well plate. The PL intensity was dramatically changed
354 as a function of the virus concentration. In the presence of the influenza virus, the PL
355 intensity showed an 8-fold increase, as compared to the corresponding intensity in

the absence of the same virus (Fig. S6). The calibration curve was obtained in the range 50–10,000 PFU/mL (Fig. 6.) and the detection limit was 50 PFU/mL. This implies that the clinically isolated virus was successfully detected by PAFI using the Ab-conjugated AuCNTs and the CdTe QDs. The selectivity of PAFI was confirmed using the anti-HA Ab (Ab66189)-conjugated AuCNTs and the CdTe QDs. The anti-HA Ab (Ab66189) could only recognize the HA present in the influenza virus (H1N1). The PL for influenza virus A/Yokohama/110/2009 (H3N2) was low, similar to that of the negative control (BSA) (Fig. S7).

4. Conclusion

In this study, the influenza virus monitoring was successfully demonstrated by interaction between plasmonic nanomaterials and fluorescent particles. In particular, novel PAFI system was developed using AuCNT and CdTe nanomaterials. To perform the PAFI, the AuCNTs were prepared by a simple 2 step-process, using a mild reducing agent without thermal assistance or harsh reducing agents. A large number of Au NPs were decorated onto the surfaces of the CNTs, and they showed a surface plasmon resonance effect at the AuCNT surface. Thus, the AuCNT surface played an important role as the plasmonic substrate for the PAFI. Various influenza viruses were monitored and the detection limits of PAFI against influenza viruses A/Beijing/262/95 (H1N1) and New Caledonia/20/99IvR116 (H1N1) were 1 ng/mL and 0.1 pg/mL, respectively. For the detection of the New Caledonia virus, two different types of antibodies were attached onto the surface of each of the nanomaterials, and then used for monitoring the virus. In this case, the detection limitation was higher than that of the single antibody system (Beijing virus detection), owing to less competitive binding affinity. In previous reports, the detection limitation for proteins

380 and viruses was reported to be approximately in the ng range (Ahmed et al. 2014; Li
381 et al. 2012;Nooney et al. 2010). As compared to the other PAFI detection systems,
382 the detection limitation for this particular system was improved by about 10-fold. The
383 clinically isolated influenza virus A/Yokohama/110/2009 (H3N2) was also tested, and
384 the corresponding sensitivity was 50 PFU/mL. The PAFI system also showed
385 excellent selectivity, which was 100-fold higher than that of the commercial
386 diagnostic kit. This system may be applied not only to the influenza virus, but also to
387 various other infectious viruses.
388

389 Acknowledgement

390 We wish to thank Dr. C. Kawakami of the Yokohama City Institute of Health,
391 Japan for providing the influenza virus A/Yokohama/110/2009 (H3N2). This work
392 was supported partly by the Promotion of Nanobio-technology Research to support
393 Aging and Welfare Society from the Ministry of Education, Culture, Sports, Science
394 and Technology, Japan. This study was supported by a grant from the Korean
395 Health Technology R&D Project, Ministry of Health & Welfare, Republic of Korea
396 (HI13C0862); and by the Basic Science Research Program through the National
397 Research Foundation of Korea (NRF), funded by the Ministry of Education
398 (2013004637).

399 Appendix. Supportinginformation

400 Supplementary data associated with this article can be found in the online
401 version.

402

403 Reference List

Ahmed SR, Dong JH, Yui M, Kato T, Lee J, Park EY. 2013. Quantum dots incorporated magnetic nanoparticles for imaging colon carcinoma cells. Journal of Nanobiotechnology 11, 28.

Ahmed RS, Hossain MA, Youn Park J, Kim SH, Lee D, Suzuki T, Lee J, Park EY. 2014. Metal enhanced fluorescence on nanoporous gold leaf-based assay platform for virus detection. Biosensors and Bioelectronics 58, 33-39.

Aruoma OI, Murcia A, Butler J, Halliwell B. 1993. Evaluation of the Antioxidant and Prooxidant Actions of Gallic Acid and Its Derivatives. Journal of Agricultural and Food Chemistry 41, 1880-1885.

Baro M, Nayak P, Baby TT, Ramaprabhu S. 2013. Green approach for the large-scale synthesis of metal/metal oxide nanoparticle decorated multiwalled carbon nanotubes. Journal of Materials Chemistry A 1, 482-486.

Draz MS, Fang BA, Li LJ, Chen Z, Wang YJ, Xu YH, Yang J, Killeen K, Chen FF. 2012. Hybrid Nanocluster Plasmonic Resonator for Immunological Detection of Hepatitis B Virus. Acs Nano 6, 7634-7643.

Gaponik N, Talapin DV, Rogach AL, Hoppe K, Shevchenko EV, Kornowski A, Eychmuller A, Weller H. 2002. Thiol-capping of CdTe nanocrystals: An alternative to organometallic synthetic routes. Journal of Physical Chemistry B 106, 7177-7185.

Georgakilas V, Gournis D, Tzitzios V, Pasquato L, Guldi DM, Prato M. 2007. Decorating carbon nanotubes with metal or semiconductor nanoparticles. Journal of Materials Chemistry 17, 2679-2694.

Gobbo P, Biesinger MC, Workentin MS. 2013. Facile synthesis of gold nanoparticle (AuNP)-carbon nanotube (CNT) hybrids through an interfacial Michael addition

reaction. Chemical Communications 49, 2831-2833.

Hirsch A. 2002. Functionalization of single-walled carbon nanotubes. Angewandte Chemie-International Edition 41, 1853-1859.

Holzinger M, Vostrowsky O, Hirsch A, Hennrich F, Kappes M, Weiss R, Jellen F. 2001. Sidewall functionalization of carbon nanotubes. Angewandte Chemie-International Edition 40, 4002.

Jana NR, Gearheart L, Murphy CJ. 2001. Seeding growth for size control of 5-40 nm diameter gold nanoparticles. Langmuir 17, 6782-6786.

Jariwala D, Sangwan VK, Lauhon LJ, Marks TJ, Hersam MC. 2013. Carbon nanomaterials for electronics, optoelectronics, photovoltaics, and sensing. Chemical Society Reviews 42, 2824-2860.

Kim J, Lee J, Lee KI, Park TJ, Kim HJ, Lee J. 2013. Rapid monitoring of CFP-10 during culture of Mycobacterium tuberculosis by using a magnetophoretic immunoassay. Sensors and Actuators B-Chemical 177, 327-333.

Lee J, Govorov AO, Dulka J, Kotov NA. 2004. Bioconjugates of CdTe nanowires and Au nanoparticles: Plasmon-exciton interactions, luminescence enhancement, and collective effects. Nano Letters 4, 2323-2330.

Lee J, Govorov AO, Kotov NA. 2005. Nanoparticle assemblies with molecular springs: A nanoscale thermometer. Angewandte Chemie-International Edition 44, 7439-7442.

Lee J, Hernandez P, Lee J, Govorov AO, Kotov NA. 2007. Exciton-plasmon interactions inmolecular spring assemblies of nanowires and wavelength-based protein detection. Nature Materials 6, 291-295.

Lee J, Kim HY, Zhou H, Hwang S, Koh K, Han DW, Lee J. 2011a. Green synthesis of phytochemical-stabilized Au nanoparticles under ambient conditions and their biocompatibility and antioxidative activity. Journal of Materials Chemistry 21, 13316-13326.

Lee J, Orazbayev A, Govorov AO, Kotov NA. 2010. Solvent Effect in Dynamic

Superstructures from Au Nanoparticles and CdTe Nanowires: Experimental Observation and Theoretical Description. Journal of Physical Chemistry C 114, 1404-1410.

Lee J, Park E, Lee J. 2014. Non-toxic nanoparticles from phytochemicals: preparation and biomedical application. Bioprocess Biosyst Eng 37, 983-989.

Lee J, Zhou H, Lee J. 2011b. Small molecule induced self-assembly of Au nanoparticles. Journal of Materials Chemistry 21, 16935-16942.

Lee YH, Polavarapu L, Gao N, Yuan P, Xu QH. 2012. Enhanced Optical Properties of Graphene Oxide-Au Nanocrystal Composites. Langmuir 28, 321–326.

Leung KCF, Xuan SH, Zhu XM, Wang DW, Chak CP, Lee SF, Ho WKW, Chung BCT. 2012. Gold and iron oxide hybrid nanocomposite materials. Chemical Society Reviews 41, 1911-1928.

Li CX, Mezzenga R. 2013. The interplay between carbon nanomaterials and amyloid fibrils in bio-nanotechnology. Nanoscale 5, 6207-6218.

Li H, Chen CY, Wei X, Qiang WB, Li ZH, Cheng Q, Xu DK. 2012. Highly Sensitive Detection of Proteins Based on Metal-Enhanced Fluorescence with Novel Silver Nanostructures. Analytical Chemistry 84, 8656-8662.

Li HQ, Cooper-White JJ. 2013. Hyperbranched polymer mediated fabrication of water soluble carbon nanotube-metal nanoparticle hybrids. Nanoscale 5, 2915-2920.

Li XL, Qin YJ, Picraux ST, Guo ZX. 2011. Noncovalent assembly of carbon nanotube-inorganic hybrids. Journal of Materials Chemistry 21, 7527-7547.

Li YX, Hong M, Qiu B, Lin ZY, Cai ZW, Chenb YT, Chen GN. 2013. A highly sensitive chemiluminescent metalloimmunoassay for H1N1 influenza virus detection based on a silver nanoparticle label. Chemical Communications 49, 10563-10565.

Liu YX, Dong XC, Chen P. 2012. Biological and chemical sensors based on graphene materials. Chemical Society Reviews 41, 2283-2307.

McAndrew CF, Baxendale M. 2013. High electrical conductance enhancement in Au-

nanoparticle decorated sparse single-wall carbon nanotube networks. Nanotechnology 24.

Nooney R, Clifford A, LeGuevel X, Stranik O, McDonagh C, MacCraith BD. 2010. Enhancing the analytical performance of immunoassays that employ metal-enhanced fluorescence. Analytical and Bioanalytical Chemistry 396, 1127-1134.

Park JH, Choi TB, Kim SW, Hur MG, Yang SD, Yu KH. 2009. A study on effective extraction of isoflavones from soy germ using the electron beam. Radiation Physics and Chemistry 78, 623-625.

Peng XH, Chen JY, Misewich JA, Wong SS. 2009. Carbon nanotube-nanocrystal heterostructures. Chemical Society Reviews 38, 1076-1098.

Sharma H, Agarwal DC, Shukla AK, Avasthi DK, Vankar VD. 2013a. Surface-enhanced Raman scattering and fluorescence emission of gold nanoparticle-multiwalled carbon nanotube hybrids. Journal of Raman Spectroscopy 44, 12-20.

Sharma P, Kukkar M, Ganguli AK., Bhasina A., Suri CR. 2013b. Plasmon enhanced fluoro-immunoassay using egg yolk antibodies for ultra-sensitive detection of herbicide diuron. Analyst 138, 4312-4320.

Sun F, Cha HR, Bae K, Hong S, Kim JM, Kim SH, Lee J, Lee D. 2011. Mechanical properties of multilayered chitosan/CNT nanocomposite films. Materials Science and Engineering A-Structural Materials Properties Microstructure and Processing 528, 6636-6641.

Viet NX, Chikae M, Ukita Y, Maehashi K, Matsumoto K, Tamiya E, Viet PH, Takamura Y. 2013. Gold-linked electrochemical immunoassay on single-walled carbon nanotube for highly sensitive detection of human chorionic gonadotropin hormone. Biosensors & Bioelectronics 42, 592-597.

Wang HT, Dong ZX, Na CZ. 2013a. Hierarchical Carbon Nanotube Membrane-Supported Gold Nanoparticles for Rapid Catalytic Reduction of p-Nitrophenol. Acs Sustainable Chemistry & Engineering 1, 746-752.

Wang JL, Chen GH, Jiang H, Li ZY, Wang XM. 2013b. Advances in nano-scaled biosensors for biomedical applications. Analyst 138, 4427-4435.

Yick S, Han ZJ, Ostrikov K. 2013. Atmospheric microplasma-functionalized 3D microfluidic strips within dense carbon nanotube arrays confine Au nanodots for SERS sensing. Chemical Communications 49, 2861-2863.

Yin PT, Kim TH, Choi JW, Lee KB. 2013. Prospects for graphene-nanoparticle-based hybrid sensors. Physical Chemistry Chemical Physics 15, 12785-12799.

Yu YY, Chen ZG, He SJ, Zhang BB, Li XC, Yao MC. 2014. Direct electron transfer of glucose oxidase and biosensing for glucose based on PDDA-capped gold nanoparticle modified graphene/multi-walled carbon nanotubes electrode. Biosensors & Bioelectronics 52, 147-152.

Zhang YF, Xu CL, Li BX, Li YB. 2013. In situ growth of positively-charged gold nanoparticles on single-walled carbon nanotubes as a highly active peroxidase mimetic and its application in biosensing. Biosensors & Bioelectronics 43, 205-210.

Zhou H, Dong JH, Deo VK, Park EY, Lee J. 2013. Detection of anti-Neospora antibodies in bovine serum by using spiky Au-CdTe nanocomplexes. Sensors and Actuators B-Chemical 178, 192-199.

Zhou H, Lee J, Park TJ, Lee SJ, Park JY, Lee J. 2012. Ultrasensitive DNA monitoring by Au-Fe3O4 nanocomplex. Sensors and Actuators B-Chemical 163, 224-232.

404

[Supplementary Information]

Plasmon-Assisted Fluoro-Immunoassay of Au Decorated CNT for Influenza Virus Monitoring

Jaewook Lee[1,5], Syed Rahin Ahmed[2,3] , Sangjin Oh[3], Jeonghyo Kim[3], Tetsuro Suzuki[4], Kaushik Parmar[5], Simon S. Park[5], Jaebeom Lee[3*], and Enoch Y. Park[1,2*]

[1] Research Institute of Green Science and Technology, Shizuoka University 836 Ohya Suruga-ku, Shizuoka 422-8529, Japan
[2] Department of Bioscience, Graduate School of Science and Technology, Shizuoka University, 836 Ohya Suruga- ku, Shizuoka 422-8529, Japan
[3] Department of Nano Fusion Engineering, and Cogno-Mechatronics Engineering, Pusan National University, Busan 609-735, Korea
[4] Department of Infectious Diseases, Hamamatsu University School of Medicine, 1-20-1 Higashi-ku, Handa-yama, Hamamatsu 431-3192, Japan
[5] Department of Mechanical and Manufacturing Engineering, University of Calgary, Calgary, T2N 1N4, Canada

ELISA for Confirmation of Ab Conjugation on the Surface of AuCNTs and CdTe QDs

After preparation of Ab-conjugated AuCNTs via EDC/NHS coupling reaction, 100 μl of 1000 times diluted anti-mouse IgG-HRP (Santa Cruz Biotechnol., CA) was added into 1 ml of Ab-conjugated nanomaterials. When anti-neuraminidase (NA) Ab (New Caledonia/20/1999/(H1N1)) was used goat anti-rabbit IgG-HRP (Immune Technology Corp., New York, NY, USA) was used for this ELISA. Subsequently, the samples were incubated at room temperature for 1 h, and then purified by centrifuge at 9170 *g* for 10 min, three times. HRP was developed with 50 μl TMBZ substrate solution (10 μg/ml TMB) and 10% H_2O_2 in 100 mM NaOAc (pH 6.0) for 5–30 min at 25°C. The reaction was quitted by adding 25 μl of 10% H_2SO_4, and then measured the absorbance at 450 nm with a reference at 655 nm using a micro plate reader

* Address correspondence to acypark@ipc.shizuoka.ac.jp (EYP) and jaebeom@pusan.ac.kr (JL).

(Model 680, Bio-Rad, Hercules, CA, USA). Anti-HA Ab (Ab66189)-, anti-NA Ab (New Caledonia/20/1999/(H1N1))- and anti-HA Ab (Ab82454)-conjugated AuCNTs, and anti-HA Ab (Ab66189)- and anti-HA Ab (Ab82454)-conjugated CdTe QDs were measured by the same protocol as above procedure.

Supplementary Figures

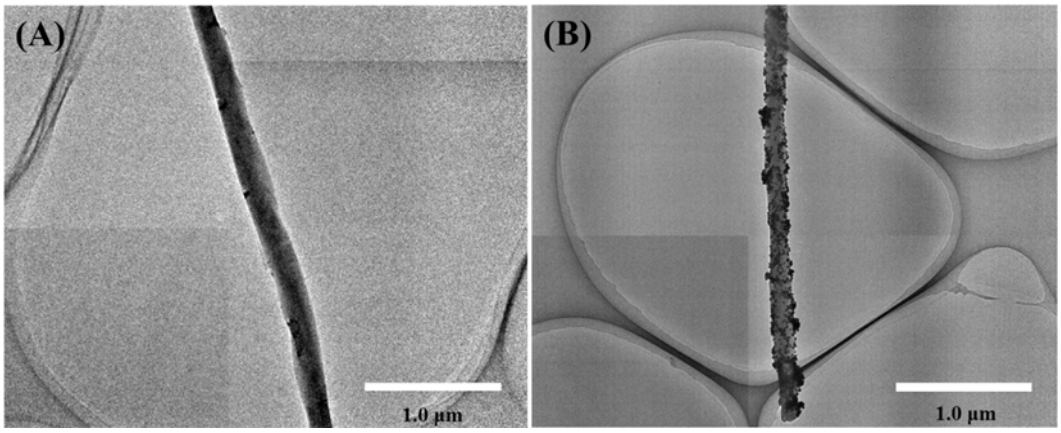

Figure S1. Low magnification TEM images of (A) MWCNT and (B) AuCNT

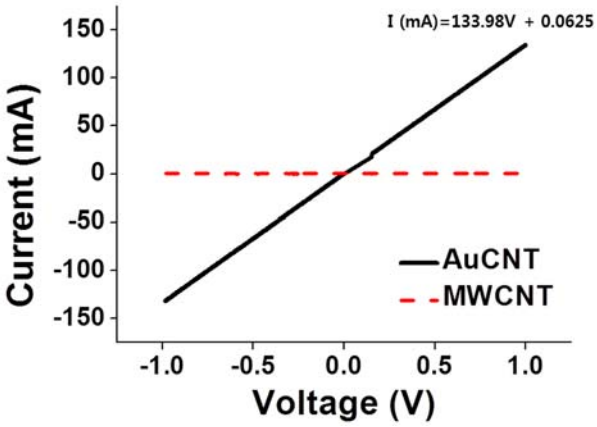

Figure S2. Line conductivity measurement: I/V curve of AuCNT and MWCNT

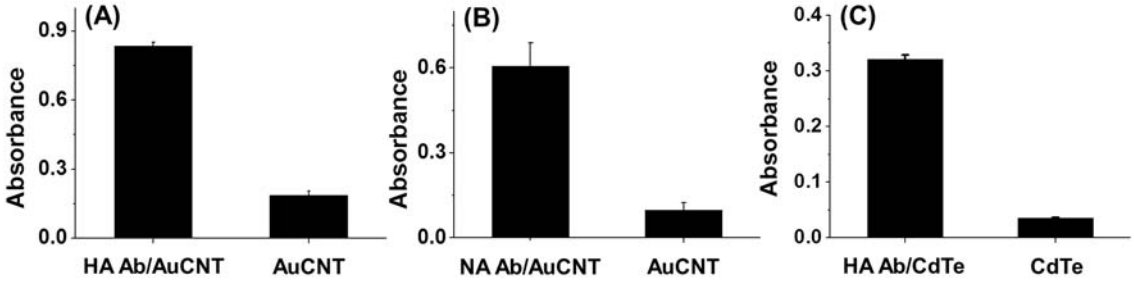

Figure S3. ELISA for confirmation of Ab conjugation on the surface of anti-HA (Ab66189) conjugated AuCNTs (A), anti-NA conjugated AuCNTs (B), and anti-HA (Ab66189) conjugated CdTe QDs (C). Error bars denote standard deviation (SD) (n=3).

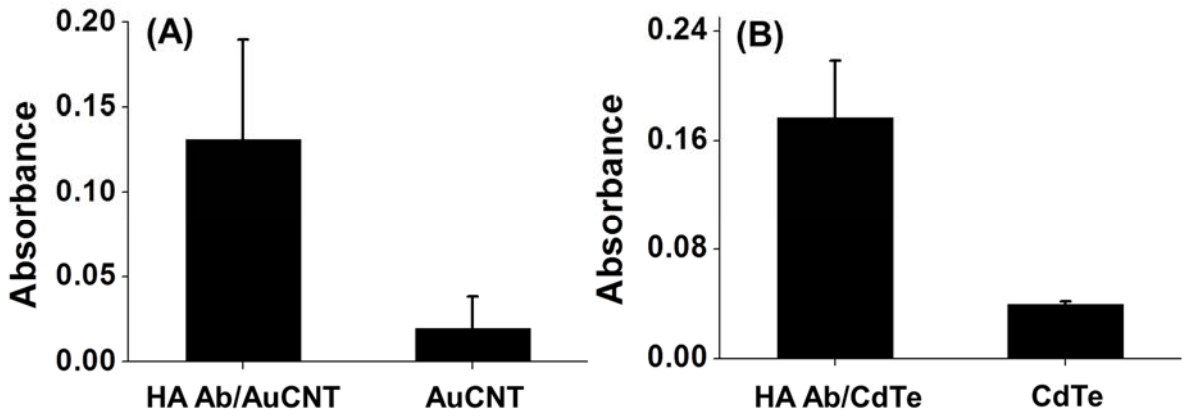

Figure S4. ELISA for confirmation of Ab conjugation on the surface of anti-HA (Ab82454) conjugated AuCNTs (A) and anti-HA (Ab82454)-conjugated CdTe QDs (B). Error bars denote standard deviation (SD) (n=3) at 450 nm.

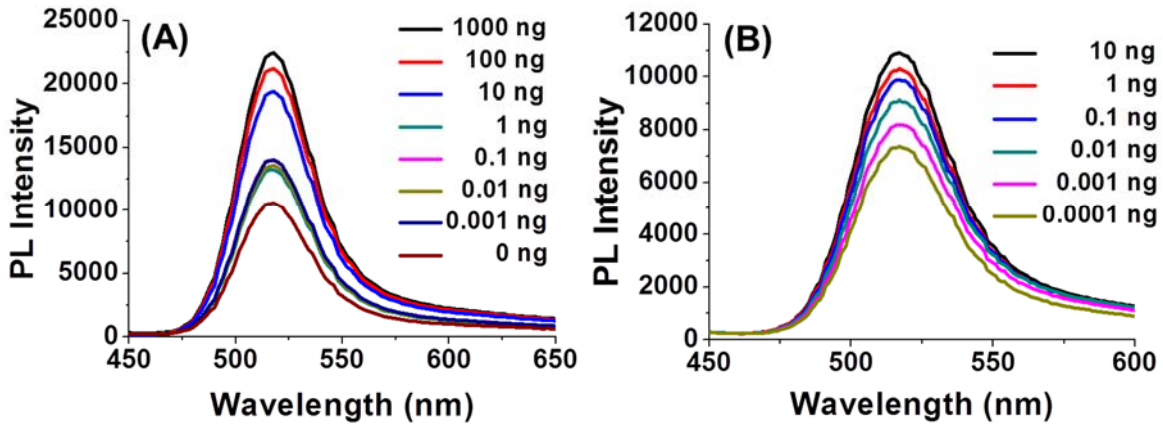

Figure S5. PL spectra monitoring for influenza virus A/Beijing/262/95 (H1N1) (A) and influenza virus/New Caledonia/20/99IvR116 (H1N1) (B).

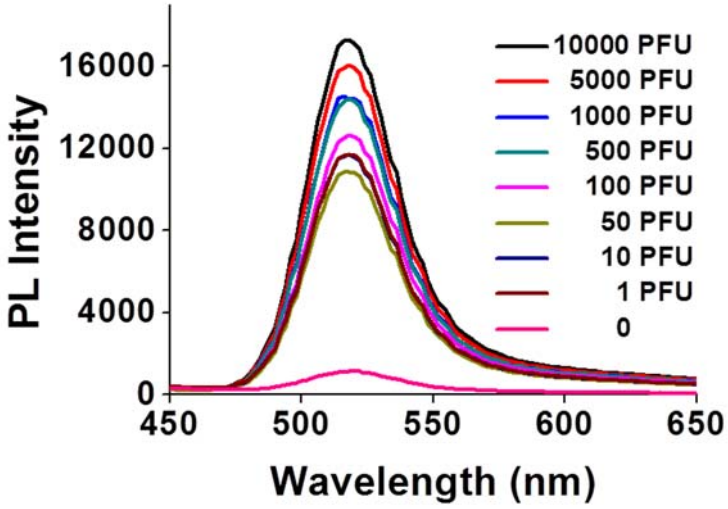

Figure S6. PL spectra of PAFI system for clinical isolated influenza virus A/Yokohama/110/2009 (H3N2)) detection.

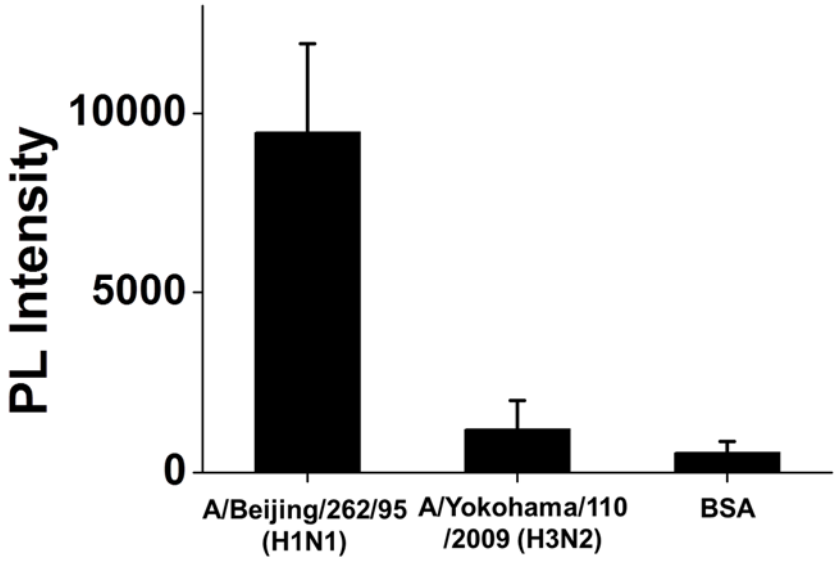

Figure S7. PL intensity monitoring for selectivity test of PAFI. When anti-HA Ab (Ab66189)-conjugated AuCNTs and CdTe QDs were used, PL intensity of influenza virus A/Beijing/262/95 (H1N1) was specifically detected, but that of influenza virus A/Yokohama/110/2009 (H3N2) was very low, similar to that of negative control (BSA).